ARTICLES
https://doi.org/10.1038/s41561-018-0139-z
nature geoscience

Thermal effects of pyroxenites on mantle melting below mid-ocean ridges

Daniele Brunelli[1,2*], Anna Cipriani[1,3*] and Enrico Bonatti[2,3]

After travelling in Earth's interior for up to billions of years, recycled material once injected at subduction zones can reach a subridge melting region as pyroxenite dispersed in the host peridotitic mantle. Here we study genetically related crustal basalts and mantle peridotites sampled along an uplifted lithospheric section created at a segment of the Mid-Atlantic Ridge through a time interval of 26 million years. The arrival of low-solidus material into the melting region forces the elemental and isotopic imprint of the residual peridotites and of the basalts to diverge with time. We show that a pyroxenite-bearing source entering the subridge melting region induces undercooling of the host peridotitic mantle, due to subtraction of latent heat by melting of the low-*T*-solidus pyroxenite. Mantle undercooling, in turn, lowers the thermal boundary layer, leading to a deeper cessation of melting. A consequence is to decrease the total amount of extracted melt, and hence the magmatic crustal thickness. The degree of melting undergone by a homogeneous peridotitic mantle is higher than the degree of melting of the same peridotite but veined by pyroxenites. This effect, thermodynamically predicted for a marble-cake-type peridotite–pyroxenite mixed source, implies incomplete homogenization of recycled material in the convective mantle.

Mantle rising beneath the 60,000-km-long mid-ocean ridge system contains, as in a slow-motion movie, a record of ancient upwelling and melting events and of interaction with subduction- or hotspot-derived components. It is difficult to reconstruct temporal records of these ancient events due to lack of suitable samples; however, we were given the opportunity to explore the temporal evolution of the oceanic lithosphere composition and structure at 11° N along the Mid-Atlantic Ridge (MAR) where an uplifted >300-km-long sliver of lithosphere exposes a basal mantle peridotite unit, lower crustal gabbros, a dyke complex and erupted basalts[1–3]. This lithospheric section (Vema lithospheric section (VLS)) was generated at an 80-km-long segment of the MAR (EMAR segment, Supplementary Fig. 1) during a 26 Myr time interval[1,2,4–6]. Both crustal basalts and their mantle peridotite parents have been densely sampled at the VLS along a seafloor spreading flow line[4] allowing comparisons of their isotopic and elemental composition throughout the 26 Myr time interval[1,2,4–6] (Fig. 1).

Surprisingly, temporal variations of the degree of melting of the mantle estimated from basalt Na_8 (refs [7,8]) anti-correlate with the degree of melting derived from spinel Cr# (Cr# = Cr/(Cr + Al)) of the peridotites[9,10], although the two curves converge to a common value in the youngest 3 Myr stretch of the VLS (Fig. 1). Older, isotopically enriched basalts display the lower Na_8 values of the entire VLS, suggesting that they were generated by a higher degree of melting of their mantle source; in contrast, the genetically associated mantle peridotites record a relatively low extent of melting, in agreement with a thinner crust recorded by geophysical data[1]. This anti-correlation contrasts with what is inferred to be the 'normal' signature of partial melting at mid-ocean ridges.

We offer a solution to this conundrum by suggesting that a subridge variably veined mantle hosts chemically enriched, fertile, low-*T*-melting components (that is, pyroxenites). Thermodynamic-based studies predict dramatic effects when pyroxenites are present in the mantle source and partially melt along a decompressive path[11–15]. Low-*T*-solidus components lower the extent of melting of the host peridotite due to subtraction of latent heat of fusion[13–15]. Pyroxenites melt preferentially, generating isotopically enriched, low-Na_8 melts and cooling the host mantle peridotites, thereby lowering the degree of melting of the peridotite mantle in proportion to its pyroxenite content[13]. Here, we account for variable extents of the melting column by assuming that different pyroxenitic contents result in a variable extent of undercooling before the ambient peridotite starts melting. This situation mimics varying the potential temperature of the mantle resulting in changes in the length of the melting column.

Evolution of crustal thickness and mantle degree of melting

Basalt Nd, Sr and Pb isotopes vary coherently along the 26-Myr-long VLS section, showing a decrease in isotopic enrichment towards younger ages that hints at temporal variations of composition and thermal state of the rising mantle[8]. We represent these variations as discrete steps (Fig. 1a), defining three time domains: 0–2 million years ago (Ma), 2–13 Ma and 13–26 Ma (Supplementary Tables 1–3).

The major element composition of the basalts also varies with age, the older samples being poorer in sodium than the younger ones. Na_8, an inverse proxy of the degree of melting experienced by the mantle column[7,8] (Supplementary Table 2), is on average lower in older basalts of the VLS; thus, they were apparently produced by a degree of melting higher than the younger basalts (Supplementary Fig. 1a). However, Na_8 has been defined for a homogeneous lherzolitic source[8]. A heterogeneous source generates complex melt mixing patterns depending on the relative extent of melting, homogenization and enrichment of each component[16–18]. For this reason, we adopt here the expression 'apparent' degree of melting.

In peridotites, the proxy equivalent (but reverse) to basalt Na_8 is the Cr# of spinels and pyroxenes[9,10]. During the last 26 Myr, peridotite spinel Cr# increased along the VLS on average from 22 to 37 (Supplementary Fig. 1c), suggesting that the amount of magma

[1]Dipartimento di Scienze Chimiche e Geologiche, Università di Modena e Reggio Emilia, Modena, Italy. [2]Istituto di Scienze Marine, CNR, Bologna, Italy. [3]Lamont Doherty Earth Observatory, Columbia University, New York, NY, USA. *e-mail: daniele.brunelli@unimore.it; anna.cipriani@unimore.it

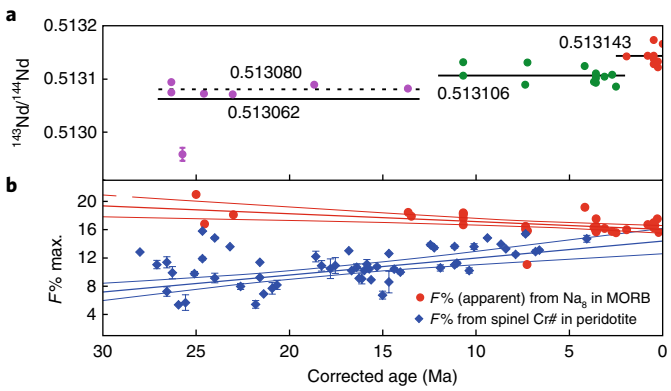

Fig. 1 | Temporal variations of Nd isotopes and degree of melting along the VLS. a, Temporal variation of the $^{143}Nd/^{144}Nd$ isotopic ratios of the VLS basaltic glasses. The filled circles define three domains (average Nd isotopic ratio of each sector is indicated). The dashed line is the average of the oldest sector without one enriched sample. **b**, Temporal variation of the degree of melting as inferred by mantle peridotite residues[19] and erupted MORBs[7]. Each point represents a dredge average. The thick bold lines are linear regressions; the thin lines show 95% confidence bands. The age of the mantle rocks is corrected for the time lag between their arrival at the seafloor and the arrival of the basaltic melts they produced according to refs[1,4] (see Methods).

delivered at the ridge axis increased through time, in agreement with gravity profiles running along spreading flow lines (Supplementary Fig. 1c), revealing that the crustal thickness increased from 4.8 ± 0.2 km in the 22–27 Ma interval to 5.4 ± 0.2 km between 0 and 5 Ma (refs[1,4]).

Based on calibrations of ref.[19], the degree of melting (F_{max}) of the VLS peridotites increased from 8.0 to 14.2 *F*% towards younger crustal ages (average 10.8, Fig. 2). The Na_8 of mid-ocean-ridge basalt (MORB) glasses increased with time along the VLS from 2.6 to 3.0 on average (Supplementary Fig. 1a). F_{max} in the basalts can be estimated according to ref.[7] and compared to the F_{max} of the mantle peridotites. Comparing temporal sections of mantle residua and of their melt products must take into account a time delay in the emplacement of the mantle peridotites in the oceanic crust. According to refs[1,4], we corrected the crustal ages of the mantle rocks relative to that of basalts by a relative time lag of 2.2 Myr (see Methods, Age correction).

The calculated apparent F_{max} values of MORB glasses vary little during the 26-Myr-long VLS stretch (Fig. 1b), with values ranging from 18.0 to 15.8 *F*% (average 16.7), significantly higher than those estimated from mantle residual peridotites (Fig. 1b). A striking feature of the Na_8 degree of melting curve is the decrease of the apparent F_{max} through time that countertrends with both the associated mantle peridotites degree of melting curve and the gravity-inferred crustal thickness (Fig. 1b and Supplementary Fig. 1c).

Significance of the decoupling

The degrees of melting estimated from the mantle peridotites and from the basalts can be generated by variations of mantle potential temperature, mantle composition and spreading rate. Changes in mantle temperature or source fertility will result in coherent changes in the degrees of melting estimated from basalts and from peridotites. Similarly, changes in spreading rate cannot decouple the behaviour of residual mantle and extracted basalts, because, in a passive upwelling scenario, decreasing the spreading rate lowers the thermal state of the entire melting region, and vice versa[20]. During the last 26 Myr, the half-spreading rate at the EMAR segment decreased from 17.2 mm yr^{-1} (Chron 6) to 16.9 mm yr^{-1} (Chron 5) to the present-day 13.6 mm yr^{-1} (refs[21,22]; Supplementary Fig. 1b). This decrease in the spreading rate towards younger ages should lower the mantle degree of melting by about 1% (ref.[20]); thus, the increase in the degree of melting recorded by the VLS mantle peridotites must be caused by processes other than changes in spreading rate, mantle temperature or fertility.

We consider now a heterogeneous mantle source. Thermodynamic modelling of melting of a two-component mantle source predicts that when a fertile heterogeneity (that is, pyroxenite) starts melting, the temperature of the whole mantle parcel is lowered due to the latent heat of melting[15]. If the heterogeneity is less than a few kilometres, some heat is transferred from the peridotite into the melting heterogeneity increasing its melt productivity while cooling the surrounding mantle[13–15]. Accordingly, the vertical interval where only pyroxenites undergo melting represents an undercooling region whose extent is proportional to the amount of pyroxenites (Fig. 2). It follows that, for a given *P*–*T* decompression path, the degree of melting undergone by a homogeneous peridotitic mantle is higher than the degree of melting of the same peridotite but veined by pyroxenites.

A lithologically homogeneous mantle source, resulting in coherent estimates of the degree of melting between peridotites and basalt proxies, is approximated in the younger (<5 Myr) portion of the VLS where both basalt- and peridotite-derived *F*% values converge towards a common value. We assume that the present-day subridge mantle (Vema unveined mantle (VUM)) contains negligible amounts of pyroxenites, not sufficient to perturb thermally the melting process of the host mantle peridotite. Thus, for this region, the Na_8-derived degree of melting is in line with its original interpretation[7,8,23].

In contrast, in a veined mantle scenario, the degrees of melting estimated from peridotites and from basalts differ strongly. While the Cr# records the true F_{max} of the ambient peridotite, the pooled melts aggregate the compositional signal of both (low *F*) peridotitic and (high *F*) pyroxenitic melts[18]. We propose that the low degree of melting of the older portion of the VLS peridotites is due to heat consumption during preferential melting of a pyroxenitic component at nearly constant mantle potential temperature. Along the VLS, we have decreasing quantities of pyroxenites injected into the melting region, with a consequent decrease of the undercooling effect and expansion of the anhydrous peridotite melting region.

We tested this hypothesis by modelling the decompressive adiabatic melting of a mixed source based on the experimentally-parameterized algorithm Melt-PX[24]. Mantle potential temperatures have been constrained using the passive-flow temperature field model of ref.[1], giving a mantle $T_p = 1{,}350$ °C. For this temperature and a lherzolitic source containing 15% clinopyroxene, Melt-PX calculations overestimate crustal thickness and mantle degrees of melting observed at the EMAR segment (Fig. 3). These calculations assume that melting ceases at the base of the crust, a boundary condition acceptable for high mantle T_p settings as in fast-spreading ridges or hotspots[24,25]. They represent the model maximum allowed thickness at a given thermal setting (Fig. 3). Mantle flow models[1,26] predict the end of melting to occur at $P_f \approx 0.7$ GPa, well below the base of the crust. This condition applies to low-spreading ridges due to heat conduction to the surface resulting in a deep transition from the conductive to the convective thermal region[20,26–28].

As low-melting component, we adopted the silica-deficient pyroxenite M7-16[29] for reasons defined in the next section. We observe that an increase in the fraction X_p of pyroxenite in the mantle is paralleled by a decrease in the degree of melting of the host peridotite (F_π) (Fig. 3) depending also on the final pressure of melting (varying in the range 0.3–1.1 GPa, Fig. 3).

Integration of the melt productivity of the host peridotite and of the pyroxenite along an adiabatic path, weighted by their relative abundance, allows estimation of the magmatic crustal thickness.

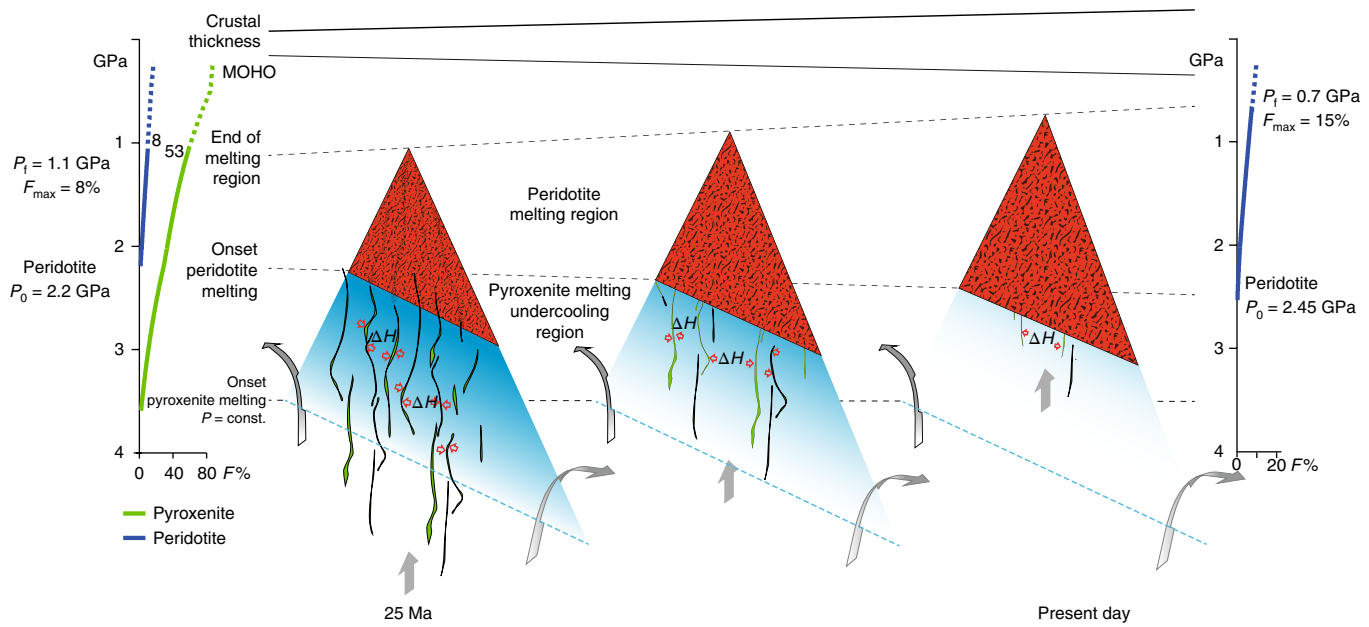

Fig. 2 | Interpretative sketch of the upwelling mantle column below the VLS. At constant mantle potential temperature, the presence of pyroxenites causes a contraction of the melting region. The total degree of decompressive adiabatic melting is computed using the Melt-PX algorithm[24]. In the older VLS sectors, the onset of melting of the mantle peridotite is delayed and its degree of melting is reduced (F_{max} = 8). The associated pyroxenite melts more (F_{max} = 53) and contributes to the higher apparent degree of melting in the pooled MORBs. Undercooling of the mantle peridotite causes deepening of the end of the melting column estimated to shallow by 0.4 GPa from the older to the younger sector.

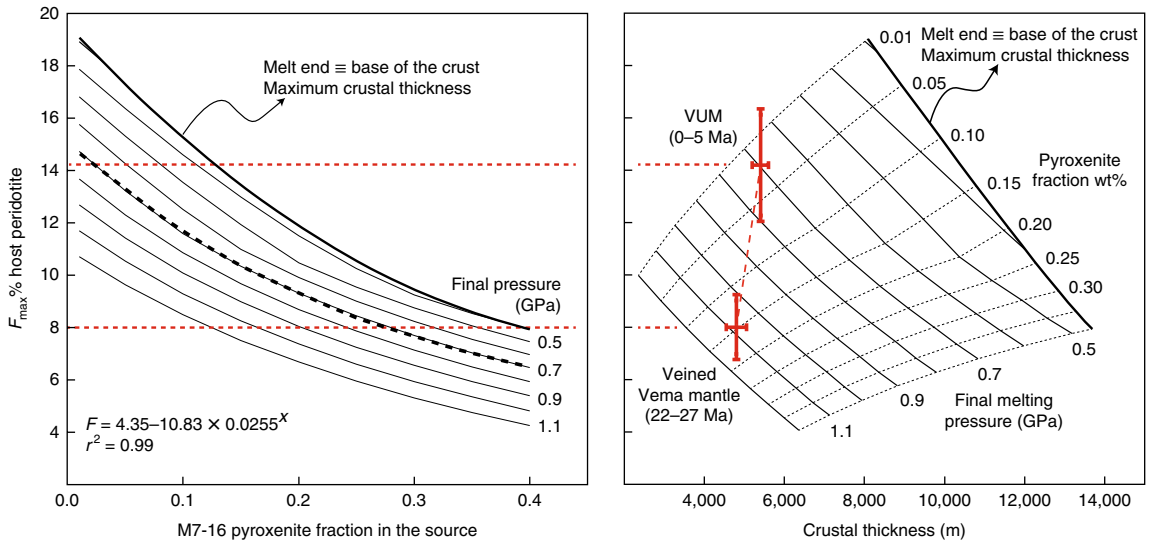

Fig. 3 | Melt-PX[24] numerical experiments for adiabatic melting of a two-component mantle source with lherzolite plus SD pyroxenite (M7-16[29]). The thick black line represents the model limit value for melting ceasing at the base of the crust. Left panel: the degree of melting of the host peridotite is lowered by adding up to 40% pyroxenite in the source. Variable extents of the melting column are computed assuming P_f from 1.1 to 0.3 GPa. The red dashed lines correspond to the VLS average melting interval from old (F_{max} = 8.0) to young (F_{max} = 14.2) sectors. Right panel: variation of the aggregated crustal thickness as a function of the pyroxenite fraction in the source and the final depth of melting. The average values for the VLS extremes are plotted as red symbols and 1σ standard deviation.

Ref. [24] shows that the total magmatic productivity increases proportionally to the amount of pyroxenite in the source. This observation apparently is in contrast with the increase towards younger ages along the VLS of gravity-inferred crustal thickness, paralleled by a decrease in the estimated amount of pyroxenites dispersed within the mantle (Fig. 2 and Supplementary Fig. 1c). This contradiction is solved by considering that increasing the amount of low-melting lithologies enhances the undercooling of the host peridotitic mantle due to heat diffusion into the melting pyroxenite[13]. Undercooling estimated by Melt-PX calculations can reach up to 40 °C for adiabatic melting under the assumed conditions. Reduced undercooling due to a decrease of the mantle pyroxenite fraction during melting results in shallowing the final pressure of melting from ≈1.1 to 0.7 GPa going from the oldest to the youngest VLS sectors (Fig. 3, right panel).

These observations and numerical experiments reveal that in slow-spreading ridges, at constant mantle potential temperature, the arrival of a pulse of pyroxenites in the mantle source region

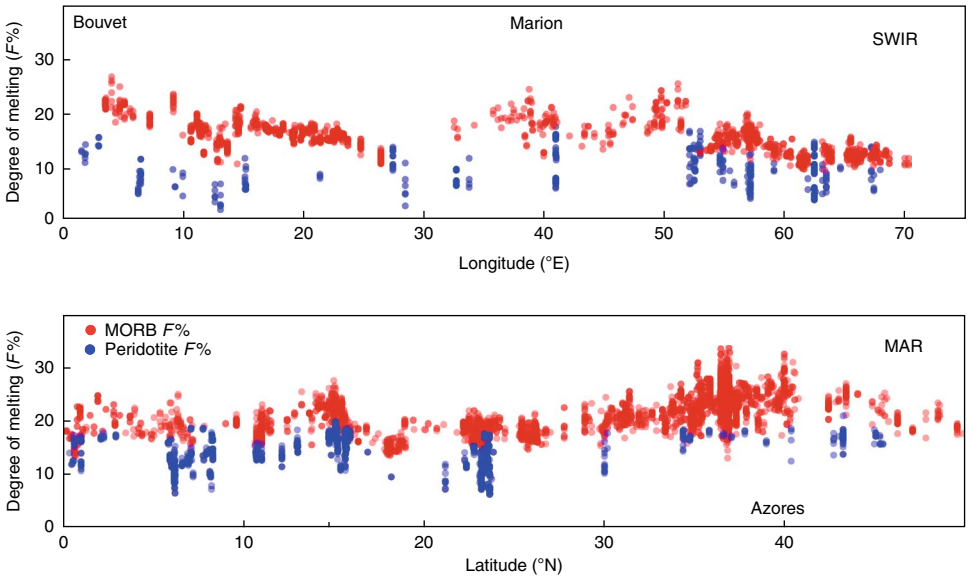

Fig. 4 | Variation of the degree of melting estimated from mantle peridotite and associated basalts along the SWIR and the MAR from the Equator to the Azores hotspot region. Degrees of melting are calculated on the basis of refs [19,23,43] on data compiled from PetDB (www.earthchem.org/petdb). Variations in the amount of low-*T*-melting heterogeneities (pyroxenite) in the source result in larger differences in the estimated degree of melting (ΔF_{π}^{β}), a proxy for the along-axis pyroxenite volume per cent content of the source.

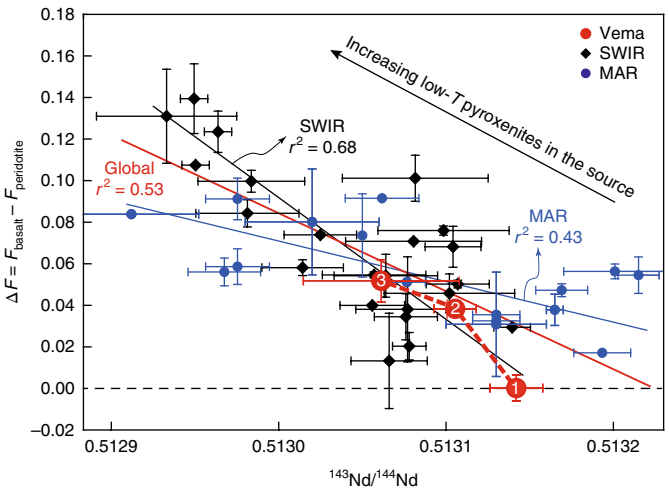

Fig. 5 | The difference in the degree of melting estimated from genetically related basalts and peridotites (Δ*F*) versus the Nd isotopic composition of basalt. The VLS sectors are plotted as large red circles; Δ*F* increases from sector 1 to 3 (young to old). The black diamonds represent the SWIR; the blue circles represent the MAR. The regression lines are calculated for the whole population (red solid line), the SWIR (black solid line) and the MAR (blue solid line). Error bars = 1σ. The data and parameters are provided in Supplementary Table 4; the 95% confidence bands are plotted in Supplementary Fig. 6. Our interpretation is that the Δ*F* between basalt and peridotite is a proxy of the amount of low-*T*-solidus pyroxenites in the source.

will cause a reduction in the crustal thickness. The countertrend of crustal thickness and degree of mantle melting with spreading rate along the VLS is a positive test of our hypothesis.

Low-solidus component composition and effects on Na_8

The effect of pyroxenite-derived melts on the final composition of the pooled MORB depends on the nature of the heterogeneities and on their dilution in the peridotite-derived melt[17,30–32]. In mid-ocean ridge settings, most pyroxenites produce melts with a major-element composition similar to those derived from peridotite[33]. Hence, little reactivity is expected when pyroxenite-derived melts mix with mantle peridotite-derived melts[34]. We thus explore the possible composition of pyroxenites dispersed in the VLS mantle by considering mixing of silica-deficient (SD) and silica-enriched (SE) pyroxenite-derived melts with peridotite-derived melts. In a Na_2O versus MgO diagram, young VLS lavas plot at higher Na_2O content than the older ones (Supplementary Fig. 2). We assume that the youngest VLS Na-rich lavas (that is, those showing a degree of melting similar to that of the associated peridotites) derive from melting of the VUM source defining a peridotite primitive melt composition that matches the VUM average Na_8 and *F*% (Supplementary Table 2). We then calculated mixing lines between the VUM primitive melt and pyroxenitic-derived melts obtained experimentally at variable degrees of melting from different sources (Supplementary Figs. 2 and 3). Melt mixing affects the estimated Na_8, and consequently the estimated apparent degree of melting, depending on the absolute Na content and Mg/Na ratio of the added melt fraction (Supplementary Fig. 3). Inferred Na_8 and apparent F of the mixed compositions show that SE-derived melts do not reproduce the observed variability for reasonable fractions and degrees of melting of the pyroxenitic-derived components (Supplementary Fig. 3). Among the SD pyroxenites, only those having high Mg/Na ratios, such as M7-16, match the VLS observed variability. It is worth noting that the mixed melts matching the VLS data are those obtained at high *F* (*F*=65%), a value close to those predicted by thermodynamics[13–15]. Based on these calculations, the VLS variability can be approximated by linear mixing of a VUM primitive melt with about 30% M7-16-type pyroxenite-derived melt.

Size and nature of mantle domains

An important result of thermodynamic modelling[13,14] is that the undercooling inferred from *F*% decoupling occurs only for a composite source where a lower-*T*-solidus component is finely dispersed in a high-*T*-solidus host to ensure efficient heat diffusion. Adopting the calibration of ref. [13] for tabular heterogeneities limits their size to be <1 km, a dimension close to those estimated from seismic

scatter (<10 km)[35]. Cryptic stripes of comparable size (4 km) have been described at the Southeast Indian Ridge[36] and modelled on the basis of Nd–Hf MORB variability[37]. The compositional trend observed along the VLS suggests a decreasing decoupling of the measured parameters. The lateral extension of the melting region reaches 300 km in the spreading direction, about 70 km along axis[26]. A single large heterogeneity in the older mantle section would have measured tens of kilometres in width, excluding efficient heat diffusion within the heterogeneity itself. We deduce that the older mantle section contained a cluster of small, tabular, low-T-solidus components as in Fig. 2, decreasing in time from about 15% to 0% of the volume.

The $^{143}Nd/^{144}Nd$ versus $^{208}Pb/^{206}Pb$ ratios of VLS basalts duplicate one of the mixing trends recognized in South Atlantic basalt suites[38,39] (Supplementary Fig. 4), suggesting that those endmembers are ubiquitous in the sub-Atlantic mantle.

The $^{143}Nd/^{144}Nd$ and $^{87}Sr/^{86}Sr$ ratios of the VLS glasses vary in a restricted range (0.51295–0.51317 and 0.70258–0.70351 respectively, Fig. 1, Supplementary Fig. 5, Methods); in contrast, mantle peridotite clinopyroxenes display a large scatter ($^{143}Nd/^{144}Nd$: 0.512024–0.513616; $^{87}Sr/^{86}Sr$: 0.702220–0.705508, age-corrected values). This different compositional scatter can be generated by chromatographic dispersion in the melting column[40] or through time by reactive melt infiltration and veining[41,42].

The oldest basalts of the VLS show the highest apparent degree of melting and the most enriched Sr–Nd–Pb isotopic signature (Supplementary Figs. 4 and 5). We suggest that their compositions reflect a larger contribution of pyroxenite-derived melts. As a result, the peridotites of the older domain are less affected by decompression melting, and record lower degrees of melting, possibly preserving their original depleted MORB mantle isotopic fingerprint. In contrast, the younger basalts of the VLS received a negligible contribution of pyroxenite-derived melts. Unfortunately, we do not have enough data on the mantle peridotites of this young VLS stretch because they are still buried below the seafloor; however the few available samples indicate that this parcel of peridotitic mantle underwent a high degree of melting.

Distribution of pyroxenites along mid-ocean ridges

We attempt now to extend our findings to other portions of the mid-ocean ridge system and interpret the chemistry of genetically related basalt/peridotite in terms of the proportion of pyroxenite dispersed in the mantle source. Only two stretches of the global mid-ocean ridge system have basalt–peridotite pairs sampled densely enough to allow first-order observations: the northern MAR and the Southwest Indian Ridge (SWIR)[19,43]. In both cases, along-axis mantle peridotites record an extent of melting systematically lower than that recorded by the associated basalts (Fig. 4).

In light of our findings, we propose that pyroxenites are widely distributed in subridge mantle sources proportionally to $\Delta F_{\pi}^{\beta} = F_{\beta}^{app} - F_{\pi}$, the difference between the degree of melting derived from basalts and that derived from peridotites (see Methods). This interpretation, if correct, should be confirmed by a correlation between the extent of ΔF_{π}^{β} and chemical indicators of the presence of pyroxenite in the source (for example, the isotopic ratios of radiogenic elements), expected to be enriched in recycled materials. A broad negative correlation appears between the measured ΔF_{π}^{β} and the basalt $^{143}Nd/^{144}Nd$ ratios (Fig. 5 and Supplementary Table 4), suggesting the dependence of the Nd isotopic composition on ΔF_{π}^{β} ($r^2 = 0.53$) and revealing similar enriching mechanisms in the two ridge systems.

Spreading rate and mantle potential temperature may not be the leading factors affecting the composition of the extracted basalts and of the residual mantle: the relative proportion of pyroxenites versus peridotites in the mantle source maybe more important. A major implication is that at constant temperature a pulse of low-melting pyroxenite entering the melting region may not lead to a pulse of magmatism because the increased undercooling of the mantle shrinks the peridotitic melting region contrasting the increase of instantaneous pyroxenite melt production.

Our results show that low-T-melting heterogeneities dispersed in the mantle source affect not only the composition of the extracted basaltic melts, but also the total extent of melting, the volume of extracted melts and, consequently, the crustal thickness.

Methods

Methods, including statements of data availability and any associated accession codes and references, are available at https://doi.org/10.1038/s41561-018-0139-z.

Received: 11 August 2017; Accepted: 25 April 2018;
Published online: 4 June 2018

References

1. Bonatti, E. et al. Mantle thermal pulses below the Mid-Atlantic Ridge and temporal variations in the formation of oceanic lithosphere. *Nature* **423**, 499–505 (2003).
2. Brunelli, D., Seyler, M., Cipriani, A., Ottolini, L. & Bonatti, E. Discontinuous melt extraction and weak refertilization of mantle peridotites at the Vema lithospheric section (Mid-Atlantic Ridge). *J. Petrol.* **47**, 745–771 (2006).
3. Bonatti, E. et al. Flexural uplift of a lithospheric slab near the Vema transform (central Atlantic): timing and mechanisms. *Earth Planet. Sci. Lett.* **240**, 642–655 (2005).
4. Cipriani, A., Bonatti, E., Brunelli, D. & Ligi, M. 26 million years of mantle upwelling below a segment of the Mid Atlantic Ridge: the Vema lithospheric Section revisited. *Earth Planet. Sci. Lett.* **285**, 87–95 (2009).
5. Cipriani, A., Brueckner, H. K., Bonatti, E. & Brunelli, D. Oceanic crust generated by elusive parents: Sr and Nd isotopes in basalt-peridotite pairs from the Mid-Atlantic Ridge. *Geology* **32**, 657–660 (2004).
6. Cipriani, A. et al. A 19 to 17 Ma amagmatic extension event at the Mid-Atlantic Ridge: ultramafic mylonites from the Vema lithospheric section. *Geochem. Geophys. Geosyst.* **10**, Q10011 (2009).
7. Plank, T. & Langmuir, C. H. Effects of the melting regime on the composition of the oceanic crust. *J. Geophys. Res.* **97**, 19749–19770 (1992).
8. Klein, E. M. & Langmuir, C. H. Global correlations of ocean ridge basalt chemistry with axial depth and crustal thickness. *J. Geophys. Res.* **92**, 8089 (1987).
9. Dick, H. J. B. & Bullen, T. Chromian spinel as a petrogenetic indicator in abyssal and alpine-type peridotites and spatially associated lavas. *Contrib. Mineral. Petrol.* **86**, 54–76 (1984).
10. Michael, P. J. & Bonatti, E. Peridotite composition from the North Atlantic: regional and tectonic variations and implications for partial melting. *Earth Planet. Sci. Lett.* **73**, 91–104 (1985).
11. Katz, R. F. & Weatherley, S. M. Consequences of mantle heterogeneity for melt extraction at mid-ocean ridges. *Earth Planet. Sci. Lett.* **335–336**, 226–237 (2012).
12. Weatherley, S. M. & Katz, R. F. Melting and channelized magmatic flow in chemically heterogeneous, upwelling mantle. *Geochem. Geophys. Geosyst.* **13**, Q0AC18 (2012).
13. Katz, R. F. & Rudge, J. F. The energetics of melting fertile heterogeneities within the depleted mantle. *Geochem. Geophys. Geosyst.* **12**, Q0AC16 (2011).
14. Phipps Morgan, J. Thermodynamics of pressure release melting of a veined plum pudding mantle. *Geochem. Geophys. Geosyst.* **2**, 1001 (2001).
15. Sleep, N. H. Tapping of magmas from ubiquitous mantle heterogeneities: an alternative to mantle plumes? *J. Geophys. Res.* **89**, 10029–10041 (1984).
16. Ito, G. & Mahoney, J. J. Flow and melting of a heterogeneous mantle: 1. Method and importance to the geochemistry of ocean island and mid-ocean ridge basalts. *Earth Planet. Sci. Lett.* **230**, 29–46 (2005).
17. Shorttle, O. Geochemical variability in MORB controlled by concurrent mixing and crystallisation. *Earth Planet. Sci. Lett.* **424**, 1–14 (2015).
18. Rudge, J. F., Maclennan, J. & Stracke, A. The geochemical consequences of mixing melts from a heterogeneous mantle. *Geochim. Cosmochim. Acta* **114**, 112–143 (2013).
19. Warren, J. M. Global variations in abyssal peridotite compositions. *Lithos* **248–251**, 193–219 (2016).
20. Bown, J. W. & White, R. S. Variation with spreading rate of oceanic crustal thickness and geochemistry. *Earth Planet. Sci. Lett.* **121**, 435–449 (1994).
21. Cande, S. C., LaBrecque, J. L. & Haxby, W. F. Plate kinematics of the South Atlantic: Chron C34 to present. *J. Geophys. Res. Solid Earth* **93**, 13479–13492 (1988).
22. Cande, S. C. & Kent, D. V. Revised calibration of the geomagnetic polarity timescale for the Late Cretaceous and Cenozoic. *J. Geophys. Res. Solid Earth* **100**, 6093–6095 (1995).

23. Langmuir, C. H., Klein, E. M. & Plank, T. in *Mantle Flow and Melt Generation at Mid-Ocean Ridges* (ed. Morgan, J. P.) 183–280 (American Geophysical Union, Washington DC, 1992).
24. Lambart, S., Baker, M. B. & Stolper, E. M. The role of pyroxenite in basalt genesis: Melt-PX, a melting parameterization for mantle pyroxenites between 0.9 and 5 GPa. *J. Geophys. Res. Solid Earth* **121**, 5708–5735 (2016).
25. Shorttle, O. & Maclennan, J. Compositional trends of Icelandic basalts: implications for short-length scale lithological heterogeneity in mantle plumes. *Geochem. Geophys. Geosyst.* **12**, Q11008 (2011).
26. Ligi, M., Cuffaro, M., Chierici, F. & Calafato, A. Three-dimensional passive mantle flow beneath mid-ocean ridges: an analytical approach. *Geophys. J. Int.* **175**, 783–805 (2008).
27. Mckenzie, D. & Bickle, M. J. The volume and composition of melt generated by extension of the lithosphere. *J. Petrol.* **29**, 625–679 (1988).
28. Shen, Y. & Forsyth, D. W. Geochemical constraints on initial and final depths of melting beneath mid-ocean ridges. *J. Geophys. Res.* **100**, 2211–2237 (1995).
29. Lambart, S., Laporte, D. & Schiano, P. Markers of the pyroxenite contribution in the major-element compositions of oceanic basalts: review of the experimental constraints. *Lithos* **160–161**, 14–36 (2013).
30. Stracke, A., Bourdon, B. & McKenzie, D. Melt extraction in the Earth's mantle: constraints from U–Th–Pa–-Ra studies in oceanic basalts. *Earth Planet. Sci. Lett.* **244**, 97–112 (2006).
31. Stracke, A., & Bourdon, B. The importance of melt extraction for tracing mantle heterogeneity. *Geochim. Cosmochim. Acta* **73**, 218–238 (2009).
32. Rubin, K. H., Sinton, J. M., Maclennan, J. & Hellebrand, E. Magmatic filtering of mantle compositions at mid-ocean-ridge volcanoes. *Nat. Geosci.* **2**, 321–328 (2009).
33. Lambart, S., Laporte, D. & Schiano, P. An experimental study of pyroxenite partial melts at 1 and 1.5 GPa: implications for the major-element composition of Mid-Ocean Ridge Basalts. *Earth Planet. Sci. Lett.* **288**, 335–347 (2009).
34. Lambart, S., Laporte, D., Provost, A. & Schiano, P. Fate of pyroxenite-derived melts in the peridotitic mantle: thermodynamic and experimental constraints. *J. Petrol.* **53**, 451–476 (2012).
35. Helffrich, G. R. & Wood, B. J. The Earth's mantle. *Nature* **412**, 501–507 (2001).
36. Graham, D. W., Blichert-Toft, J., Russo, C. J., Rubin, K. H. & Albarede, F. Cryptic striations in the upper mantle revealed by hafnium isotopes in southeast Indian ridge basalts. *Nature* **440**, 199–202 (2006).
37. Liu, B. & Liang, Y. The prevalence of kilometer-scale heterogeneity in the source region of MORB upper mantle. *Sci. Adv.* **3**, e1701872 (2017).
38. Hoernle, K. et al. On- and off-axis chemical heterogeneities along the South Atlantic Mid-Ocean-Ridge (5-11°S): shallow or deep recycling of ocean crust and/or intraplate volcanism? *Earth Planet. Sci. Lett.* **306**, 86–97 (2011).
39. Paulick, H., Münker, C. & Schuth, S. The influence of small-scale mantle heterogeneities on Mid-Ocean Ridge volcanism: evidence from the southern Mid-Atlantic Ridge (7°30′S to 11°30′S) and Ascension Island. *Earth Planet. Sci. Lett.* **296**, 299–310 (2010).
40. Liang, Y. Simple models for dynamic melting in an upwelling heterogeneous mantle column: analytical solutions. *Geochim. Cosmochim. Acta* **72**, 3804–3821 (2008).
41. Borghini, G. et al. Meter-scale Nd isotopic heterogeneity in pyroxenite-bearing Ligurian peridotites encompasses global-scale upper mantle variability. *Geology* **41**, 1055–1058 (2013).
42. Borghini, G. et al. Pyroxenite layers in the Northern Apennines' upper mantle (Italy)-generation by pyroxenite melting and melt infiltration. *J. Petrol.* **57**, 625–653 (2016).
43. Gale, A., Langmuir, C. H. & Dalton, C. A. The global systematics of ocean ridge basalts and their origin. *J. Petrol.* **55**, 1051–1082 (2014).

Acknowledgements

This work has been supported by Italian-PRIN prot. 2015C5LN35 and by the US National Science Foundation under grant no. OCE-05-51288. We are also grateful for the support of the Deep Energy community of the Carbon Observatory funded by the Alfred P. Sloan Foundation. We thank C. Langmuir, H. Dick, J. Warren and M. Seyler for stimulating insightful discussions and critical reading of an early version of the work. We are grateful to M. Ligi for his support on geophysics and S. Lambart for helping on Melt-PX. We also thank S. Lambart and A. Stracke for their constructive reviews that greatly improved the manuscript. This is Lamont-Doherty contribution number 8205.

Author contributions

D.B. performed the modelling. A.C. analysed the samples. D.B. and A.C. processed the geochemical data and jointly wrote the paper. E.B. provided the opportunity and support for sea expeditions and work. All of the authors discussed the results and the interpretations.

Competing interests

The authors declare no competing interests.

Additional information

Supplementary information is available for this paper at https://doi.org/10.1038/s41561-018-0139-z.

Reprints and permissions information is available at www.nature.com/reprints.

Correspondence and requests for materials should be addressed to D.B. or A.C.

Publisher's note: Springer Nature remains neutral with regard to jurisdictional claims in published maps and institutional affiliations.

Methods

Analytical methods. *Major elements.* Major elements on mineral phases were collected with the electron probe (Cameca SX100) at the American Museum of Natural History (NY) using a 15 kV acceleration voltage, a 20 nA beam, a 10-μm-diameter beam and 30 s counting times. Sodium, potassium and chlorine were run under different conditions to attain a higher precision and monitor their mobility, with a 5 nA beam and counting times of 80 s. A subset of samples has been analysed with a Cameca X-Five microprobe at the CAMPARIS micro-analytical centre (University of Paris VI), following procedures detailed in ref. [44]. A number of primary mineral standards were used, as well as the MORB JDF-D2 standard.

Isotope ratios. For isotopic determinations, 50 to 250 mg of basaltic glass and clinopyroxene separate were prepared by grinding, sieving and hand-picking under a binocular microscope. Glass chips were leached in 8 N HNO_3. Clinopyroxenes were treated with three leachates to eliminate the effects of seawater alteration[5,45]. Pb was separated using AG1-X8 anion resin, Sr was separated using Eichrom Sr resin and Nd was separated in a two-column procedure using Eichrom TRU-spec resin to separate the rare-earth elements, followed by α-hydroxy isobutyric acid. Isotopes were measured on a VG Sector 54 multicollector mass spectrometer housed at the Lamont Doherty Earth Observatory of Columbia University. Sr and Nd isotopes were measured in multidynamic mode. The mass fractionation corrections were based on $^{86}Sr/^{88}Sr = 0.1194$ and $^{146}Nd/^{144}Nd = 0.7219$. Over the period of the analytical work, repeated analyses yielded a $^{87}Sr/^{86}Sr$ ratio of 0.710271 ± 0.000015 for the NBS-987 Sr standard (2σ external reproducibility, $n > 22$) and a $^{143}Nd/^{144}Nd$ ratio of 0.512096 ± 0.000023 for the JNdi-1 (2σ external reproducibility, $n > 38$). Total blanks for Sr and Nd did not exceed 80 pg. Pb data on basaltic glasses were collected in static mode, using the double-spike technique with the calibrated 207/204 spike. Replicate analyses of the Pb isotope standard NBS981 gave an average of 16.9317 ± 0.0022, 15.4912 ± 0.0027 and 36.7060 ± 0.0066 for $^{206}Pb/^{204}Pb$, $^{207}Pb/^{204}Pb$ and $^{208}Pb/^{204}Pb$, respectively. These measured Pb isotope ratios were corrected to the values defined by ref. [46] of 16.9356, 15.4891 and 36.7006, respectively, for NBS 981. Reproducibility for NBS981 is 130, 174 and 181 ppm (2σ, $n = 47$), for $^{206}Pb/^{204}Pb$, $^{207}Pb/^{204}Pb$ and $^{208}Pb/^{204}Pb$ ratios, respectively. Pb blanks measured were below 100 pg and thus negligible relative to the amount of sample analysed.

Estimate of the ΔF_{π}^{β} and $^{143}Nd/^{144}Nd$ of the associated basalts. Figure 4 reports the correlation between ΔF_{π}^{β}, as the differential in degree of melting between basalt and peridotites, and the Nd isotopic composition of basalts of several portions of the mid-ocean ridge system where both basalts and peridotites have been sampled. Among all of the explored ridge segments, only few localities report basalts and mantle peridotites sampled in the same dredge haul or site. Basaltic rocks are generally more abundant and present a much denser lateral sampling than mantle peridotites. Basalt chemistry and isotopic ratios appear to vary systematically over variable length scales, defining domains in which they show little variability or monotonic changes along the ridge axis (for example, refs [43,47,48] among others). Domains characterized by reduced variability of the chemical character of the basalts are usually bounded by major transform faults, which also act as thermal barriers[47,49–51]. Therefore, in Fig. 4, we have chosen to integrate the data set of the sites where peridotites and basalts were sampled together with sites where only mantle rocks were recovered, but for which it is possible to infer the isotopic composition of the associated basalts from the regional variability. As a conservative approach, we considered only those domains in which lateral isotopic and compositional variability is very low or described by simple monotonic trends.

The degree of melting of mantle peridotites can be affected by Cr# fluctuations due to melt–rock interaction that modify spinel[9] and pyroxene compositions[52]. Therefore, we filtered spinel composition and applied a threshold of $TiO_2 < 0.15$ wt% as discussed previously[2,19].

Supplementary Table 4 reports the inferred values, showing the measured and calculated value for each basalt–peridotite couple. The 'regional regression' data are calculated considering sets of neighbouring peridotites and basalts, whereas the 'local average' set of data refers to basalts and peridotites sampled from the same site. $\pm\sigma$ on ΔF_{π}^{β} are estimated by error propagation.

Age correction. Basalts from the VLS were erupted over a time range of 26 Myr. We applied, hence, an age correction for radiogenic ingrowth since the closure of the system to allow comparisons of their initial isotopic composition, which is controlled only by the source. The correction time should be calculated since the closure of the system, represented by the moment of separation between the source and the melt at depth, assuming there was no significant melt–rock interaction thereafter. This is attested by mantle residual rocks from the VLS being all equilibrated in the spinel field showing no late interaction with melts. The only report of plagioclase-equilibrated mantle rocks concerns the strain-driven formation of plagioclase in fertile lherzolites during mylonitization[53]. We identify the melt–source separation at the estimated upper limit of melting as inferred by modelling with Melt-PX (see the main text).

The end of the melting column can be constrained on the basis of the correlation with the measured crustal thickness and the degree of melting of the residual mantle. For the time stretch relative to the VLS, the end of the melting column can be set at 1.1 GPa for the older domain and 0.7 GPa for the younger domain. On the basis of the Africa–South America Euler vectors of ref. [21] and the geomagnetic timescale of ref. [22], the spreading rate at the EMAR axis can be estimated through time. As shown in Fig. 1, the spreading rate decreased steadily in the last 30 Myr. The absolute value decreases from 17.2 to 16.9 mm yr^{-1} at Chron 6 (half-spreading rate) and from 16.9 to 13.6 mm yr^{-1} at Chron 5. Crustal ages can be calculated accordingly during this time stretch assuming that basalts erupted in the axial region.

The times of extraction for the mantle residue and for the basalts are, however, very different. Ascent rates for the basaltic liquids are estimated in the range of metres per year[54–56]. Setting the melt–source separation at 1.1 and 0.7 GPa and upwelling rates in the range 1–5 m yr^{-1} (ref. [56]) gives upwelling times ranging from 7 to 36 kyr for the older VLS domain and 5 to 23 kyr for the younger VLS domain. Such delays are uninfluential in the age correction of long-time decay systems such as those discussed here (Sm–Nd; Rb–Sr; U–Pb); however, we considered this contribution for the total age correction when discussing age-corrected values in Fig. 1b and Supplementary Fig. 1.

Upwelling of the mantle lasts a significant amount of time and can sensibly modify the isotopic relationships. The time necessary for a mantle parcel to join the crust from the top of the melting column is 2.1 Myr for the older VLS domain and 1.7 Myr for the younger VLS domain.

Code availability. The code used to calculate adiabatic melting of a two-component mantle source, Melt-PX[24], can be accessed at https://agupubs.onlinelibrary.wiley.com/doi/abs/10.1002/2015JB012762.

Data availability. The raw data are available in the Supplementary Information and in the PetDB data repository (http://www.earthchem.org/petdb).

References

44. Seyler, M. & Brunelli, D. Sodium chromium covariation in residual clinopyroxenes from abyssal peridotites sampled in the 43°–46°E region of the Southwest Indian Ridge. *Lithos* **302–303**, 142–157 (2018).
45. Cipriani, A., Bonatti, E. & Carlson, R. W. Nonchondritic ^{142}Nd in suboceanic mantle peridotites. *Geochem. Geophys. Geosyst.* **12**, Q03006 (2011).
46. Todt, W., Cliff, R., Hanser, A. & Hofmann, A. W. Evaluation of a 202Pb–205Pb double spike for high-precision lead isotope analysis. *Geophys. Monogr. Ser.* **95**, 429–437 (1996).
47. Meyzen, C. M. et al. New insights into the origin and distribution of the DUPAL isotope anomaly in the Indian Ocean mantle from MORB of the Southwest Indian Ridge. *Geochem. Geophys. Geosyst.* **6**, Q11K11 (2005).
48. Meyzen, C. M., Toplis, M. J., Humler, E., Ludden, J. N. & Mevel, C. A discontinuity in mantle composition beneath the southwest Indian ridge. *Nature* **421**, 731–733 (2003).
49. Cannat, M., Rommevaux-Jestin, C., Sauter, D., Deplus, C. & Mendel, V. Formation of the axial relief at the very slow spreading Southwest Indian Ridge (49° to 69°E). *J. Geophys. Res.* **104**, 22825–22843 (1999).
50. Seyler, M., Brunelli, D., Toplis, M. J. & Mével, C. Multiscale chemical heterogeneities beneath the eastern Southwest Indian Ridge (52°E–68°E): Trace element compositions of along-axis dredged peridotites.*Geochem. Geophys. Geosyst.* **12**, Q0AC15 (2012).
51. Paquet, M., Cannat, M., Brunelli, D., Hamelin, C. & Humler, E. Effect of melt/mantle interactions on MORB chemistry at the easternmost Southwest Indian Ridge (61°–67°E). *Geochem. Geophys. Geosyst.* **17**, 4605–4640 (2016).
52. Brunelli, D., Paganelli, E. & Seyler, M. Percolation of enriched melts during incremental open-system melting in the spinel field: a REE approach to abyssal peridotites from the Southwest Indian Ridge. *Geochim. Cosmochim. Acta* **127**, 190–203 (2014).
53. Cannat, M. & Seyler, M. Transform tectonics, metamorphic plagioclase and amphibolitization in ultramafic rocks of the Vema transform fault (Atlantic Ocean). *Earth Planet. Sci. Lett.* **133**, 283–298 (1995).
54. Spiegelman, M. & Kenyon, P. The requirements for chemical disequilibrium during magma migration. *Earth Planet. Sci. Lett.* **109**, 611–620 (1992).
55. Spiegelman, M. & Elliott, T. Consequences of melt transport for uranium series disequilibrium in young lavas. *Earth Planet. Sci. Lett.* **118**, 1–20 (1993).
56. Lundstrom, C. C., Gill, J., Williams, Q. & Perfit, M. R. Mantle melting and basalt extraction by equilibrium porous flow. *Science* **270**, 1958–1961 (1995).